Selective heavy metal removal and water purification by microfluidically-generated chitosan microspheres: Characteristics, modeling and application

Bingjie Wang[a,b], Zhishan Bai[a,*], Haoran Jiang[c], Pepijn Prinsen[b], Rafael Luque[b], Shuangliang Zhao[c], Jin Xuan[d,*]

[a] State Environmental Protection Key Laboratory of Environmental Risk Assessment and Control on Chemical Process, School of Mechanical and Power Engineering, East China University of Science and Technology, Shanghai 200237, P. R. China

[b] Departamento de Química Orgánica, Universidad de Córdoba, Edif. Marie Curie, Ctra Nnal IV-A, Km 396, E14014 Córdoba, Spain

[c] State Key Laboratory of Chemical Engineering, School of Chemical Engineering, East China University of Science and Technology, Shanghai 200237, P. R. China

[d] Department of Chemical Engineering, Loughborough University, Loughborough, LE11 3TU, United Kingdom

[*]Corresponding Authors, Email addresses: baizs@ecust.edu.cn (Z. Bai), j.xuan@lboro.ac.uk (J. Xuan). Tel: +44 (0) 1509227186; Fax: +44 (0)1509 222533.

Abstract

Many industrial wastewater streams contain heavy metals, posing serious and irreversible damage to humans and living organisms, even at low concentrations due to their high toxicity and persistence in the environment. In this study, high-performance monodispersed chitosan (CS) microspheres were prepared using a simple microfluidic method and evaluated for metal removal from contaminated water. Batch experiments were carried out to evaluate the adsorption characteristics for the removal of copper ions, one representative heavy metal, from aqueous solutions. The inherent advantages of microfluidics enabled a precise control of particle size (CV=2.3%), while exhibiting outstanding selectivity towards target ions (adsorption capacity 75.52 mg g^{-1}) and fair regeneration (re-adsorption efficiency 74% after 5 cycles). An integrated adsorption mechanism analytic system was developed based on different adsorption kinetics and isotherms models, providing an excellent adsorption prediction model with pseudo-second order kinetics (R^2 = 0.999), while the isotherm was fitted best to the Langmuir model (R^2 = 0.998). The multi-step adsorption process was revealed via quantitative measurements and schematically described. Selective adsorption performance of CS microspheres in the present of other competitive metal ions with different valence states has been demonstrated and studied by both experimental and density functional theory (DFT) analysis.

Keywords: wastewater treatment; selective heavy metal ions removal; microfluidic technology; CS microspheres; integrated adsorption mechanism analytic system; DFT analysis.

1. Introduction

Heavy metals represent a serious and exposure risk to the environment and actually are still prominent in industrial wastewaters [1, 2]. The highly toxic nature and long persistence of these metals, such as lead (Pb), cobalt (Co), copper (Cu) and manganese (Mn), can cause serious health effects to flora and fauna. Excessive intake or long term exposure (accumulation effect) to toxic heavy metals will contribute to unexpected and irreversible physical health issues to humans, such as nervous system disorders, acute poisoning, as well as multi-organ failure [3-6]. Today, the removal of metal ions from industrial wastewaters remains problematic. Various techniques can be applied for the removal of heavy metals, including spray-drying [7], precipitation polymerization [8], ion-exchange [9], electrochemical reaction [10], reverse osmosis and adsorption [11, 12]. Adsorption is considered as one of the most cost-effective methods, considering investment costs, energy consumption, throughput capacity, emission standards and toxic by-products generation [13]. Combining adsorption with other methods, toxic heavy metal ions can be efficiently eliminated and/or effectively recovered from wastewaters.

Chitosan (CS) has great potential for heavy metal adsorption based on some distinct advantages, including non-toxicity, biocompatibility and biodegradability [14, 15]. CS is also a versatile material, due to the enrichment of hydroxyl and amino active functional groups, opening the possibility of various chemical modifications, such as acylation, chelation, graft copolymerization and crosslinking. Unfortunately, CS is known to be very sensitive to changes in pH resulting in dissolution or partial transformation to gel state [16]. Poor mechanical

properties of CS powder or flakes can cause difficulties in separation and make it unsuitable for actual industrial applications.

Recently, microfluidic technology is increasingly applied and further developed, aiming to provide a precise control of the final particle morphology and monodispersity, with controllable sizes and various structures. CS particles synthesized by microfluidical technologies have shown tremendous potential in wastewater treatment [17-20]. Cu for example, as a representative and abundant metal, was used in various adsorptive removal studies. In order to evaluate the adsorption performance of microfluidically-generated adsorbents, pseudo-first order and -second order models for adsorption kinetics and Langmuir and Freundlich equations for adsorption isotherms are often utilized. Although several attempts were reported to date for the removal of Cu from contaminated water using microfluidically-generated CS microspheres, it still lacks an integrated adsorption system to quantitatively analyze the complex adsorption process. Xu et al. [18] prepared monodispersed CS microspheres using in-house built microfluidic chips, which showed an adsorption capacity of 52 mg g^{-1}, according to the non-holonomic system used to study the Cu uptake process. Zhu et al. [21] introduced a multi-step microfluidic synthesis procedure using an imprinted method to obtain CS microspheres, exhibiting enhanced Cu adsorption capacity (81 mg g^{-1}), improving the capacity found (42 mg g^{-1}) in their previous works using conventionally prepared CS microspheres [22]. Again, the same non-holonomic system could not fully describe the adsorption process. Although the increased adsorption performance of CS microspheres have been achieved by combining the microfluidic technology and chemical modification, as shown in recent research works [18, 23-25]. Still, the analysis method used to describe the complex adsorption mechanism have room for improvement.

In order to address these findings, the present study reports novel CS microspheres prepared by a one-step microfluidic method, and aims to introduce an integrated adsorption analytic system to systematically study the Cu adsorption mechanism and evaluate the adsorbents' performances more thoroughly. The CS microspheres were characterized, including their size, dispersity, adsorption capacity, selectivity and re-usability. The multi-step adsorption process was analyzed in an unprecedented way by confirming the quantitative measurements and models. The mechanism of selective adsorption was well explained by incorporating ionic scale effect and density functional theory (DFT) analysis. This work aims to further optimize the preparation of CS-based microspheres for application in metal contaminated wastewater treatment and improve the evaluation method of pollutant adsorbents.

2. Experimental

2.1. Materials and characterizations

All reagents were analytical grade and used as received. Characterizations of CS microspheres were systematical analyzed by furrier transmission infrared spectroscopy (FT-IR), scanning electron microscope (SEM) and energy dispersive X-ray spectroscopy (EDX). More details involved in this work can be found in Supporting Materials (SI).

2.2. Preparation of monodisperse CS microspheres

To prepare CS microspheres, the dispersed phase (an aqueous solution containing 4.0 wt% chitosan and 2.0 wt% acetic acid) and the continuous phase (*n*-octanol solution with 2.0 wt% Span80) were injected into the microfluidic chip by 2 syringe pumps (Longer LSP01-1B). In the flow-focusing channel of homemade microfluidic chip (**Fig.1a-c** and **Fig.S1**), the dispersed phase was continuously sheared by the continuous phase from side channels to generate a series

of chitosan emulsion templates. The as-prepared templates were collected and cross-linked in a solidification bath (*n*-octane solution with 0.5 wt% glutaraldehyde and 2.0 wt% Span80) with gentle magnetic stirring (ZNCL-S-10D), through Shiff-base reaction between glutaraldehyde and CS (**Fig.1d**). Eventually, CS microspheres were thoroughly washed sequentially with acetone, ethanol and copious amounts of deionized water to remove the remaining impurities on the microsphere surface before drying under vacuum (DHG-9023A, 40 °C, 3 h). An overview of the synthesis process is illustrated in **Fig.1e**.

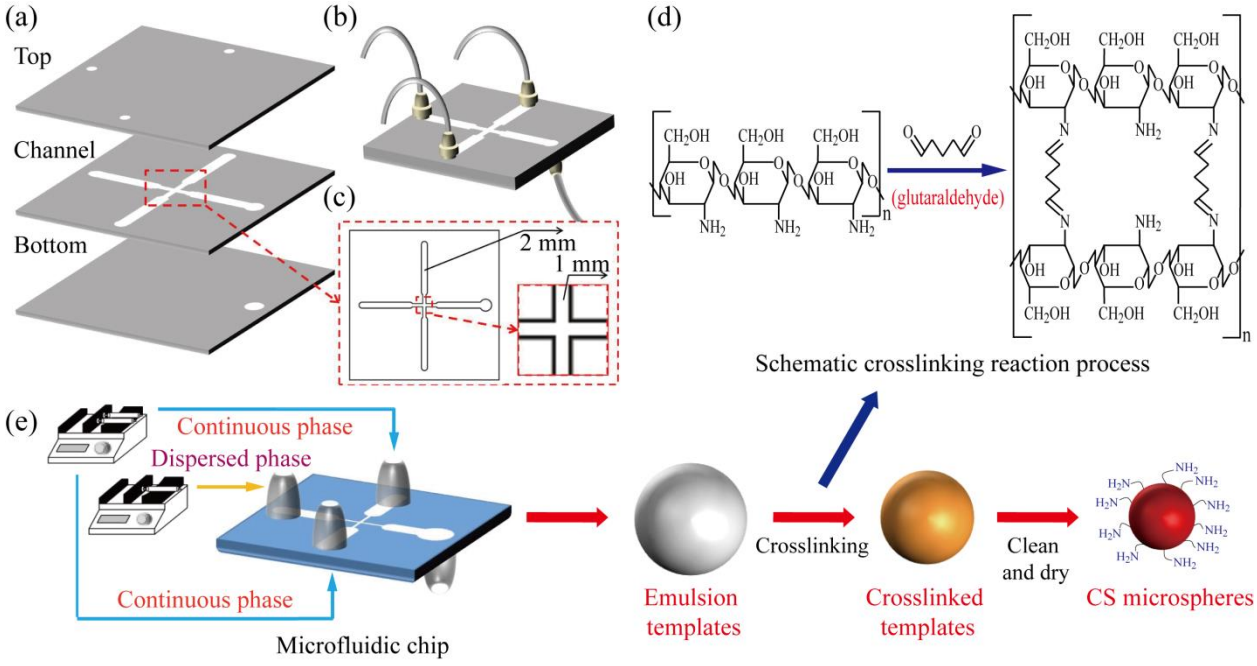

Fig.1. Schematic illustration of the microfluidic chip: (a) layer structure; (b) assembly; (c) flow-focusing junction; (d) Cross-linking process; (e) Overview of the synthesis process of CS microspheres.

2.3. Performance experiments

Cu ions as the adsorbed target was used in the batch adsorption experiments. The adsorption experiments were carried out in duplicate. Besides, the strong competition of adsorption sites

between Cu and other metal ions was also taken into consideration. For batch adsorption experiments, a Cu ion solution was first prepared by dissolving $CuCl_2 \cdot 2H_2O$ (Sinopharm Chemical Reagent Co., Ltd) in deionized water, which was further diluted to a target concentration. Subsequently, 0.05 g of CS microspheres was added to 40 mL of a Cu solution. The experiments were performed at 35 °C in an incubator (SPH-304) under constant shaking at 160 rpm. In terms of cross-linking degree of as-prepared CS microspheres and solution original pH effect of final absorbance, subsequent adsorption experiments were conducted at pH = 5.5 by using the CS microspheres with 30 min. solidification time unless otherwise stated. A fixed volume of solution was taken out at fixed time intervals and analyzed by the inductively coupled plasma optical emission spectrometer with radial views (ICP-OES, Agilent ICP-725ES). The adopted instrument operational conditions are summarized in **Table S1**.

The equilibrium adsorption capacity was calculated using the following equation:

$$q_e = \frac{(C_0 - C_e)V_0}{m} \quad (1)$$

where C_0 (ppm) and C_e (ppm) are the initial and equilibrium concentration of Cu ions in the solution, respectively. V_0 is initial volume of the solution (L) and m is the adsorbent dosage (g). The adsorption kinetics and adsorption isotherms are evaluated in Section 3.2 and 3.3. The selectivity towards Cu ions was also systematically studied by introducing different valence states of metal ions, *i.e.*, Na and Al ions, which are abundant in natural water sources (such as sea, river and mineral water). Besides, the selective adsorption performance of as-prepared CS microspheres towards Cu ions in the co-existence of other competitive metal ions with bivalence state, including Co and Mn ions, were also explored in detail.

Adsorption thermodynamics experiments were conducted by analyzing a certain volume of solution taken out after equilibrium adsorption with different initial concentrations varying from 50 to 500 ppm. The adsorption equilibrium time was defined by adsorption kinetics experiment. Additionally, the experimental details to evaluate the regeneration performance of as-prepared CS microspheres are presented in SI.

2.4. DFT calculation

The quantum chemical simulation of the investigated molecular fragments (built in Materials Studio program) within the frames of density functional theory (DFT) was carried out using Gaussian 09 [26] program package with hybrid functional B3LYP/6-311+G(d,p) [27, 28] and LanL2DZ [29]. A simplified DFT calculation was introduced to investigate the interaction of different metal ions with as-prepared CS microspheres (For more details, see SI). All studied complexes and chitosan monomer were modeled and optimized to lower energy conformation at the hybrid function B3LYP and 6-311+G(d,p) basis sets. After optimization and characterization of adsorbents, investigated metal ions were placed over different spatial locations of chitosan to study the possible complexes formed. Metal ion-adsorbent complexation was performed and optimized at B3LYP/LanL2DZ level of theory [30]. The adsorption energy (ΔE) of adsorbent-metal ions can be calculated as follows [31]:

$$\Delta E = E_{complex} - [E_{adsorbent} + E_{metal\ ion}] \quad (2)$$

where $E_{complex}$, $E_{adsorbent}$ and $E_{metal\ ion}$ are the calculated total energies (kJ mol^{-1}) of metal complex, as-prepared CS microspheres and metal ions, respectively.

3. Results and discussion

3.1. Characterization of CS microspheres

A typical adsorption experimental procedure is illustrated in **Fig.2a**. The morphology change was studied by comparing as-prepared CS microspheres and the ones recovered after the adsorption process. Under an optical microscope, a remarkable size uniformity, high monodispersity and sphericity of CS templates were observed (**Fig.2b**), as a result of the microfluidic production process. This is supported by the corresponding SEM images of a certain amount of CS microspheres (**Fig.2g**). The average diameters of CS emulsion templates after 30 min. cross-linking and as-prepared CS microspheres were 940.4 μm (CV = 0.27%) and 378.2 μm (CV = 2.3%), respectively. The specific surface area of the adsorbent tested by BET method was 6.14 m^2 g^{-1}. Distinguished morphology properties are undoubtedly convenient for industrial separations, which require a high degree of control over microparticles at the process level. With an appropriate level of chitosan content and the flow ratio of 2 phases change, the precise control towards CS templates sizes could be easily achieved (for details, see SI **Fig.S2**). Additionally, the SEM images of the surface and inner structures of single CS microsphere demonstrated its solid spherical structure as presented in **Fig.2e and f**. When reaching the adsorption equilibrium, the color of the CS microspheres turned from reddish brown (**Fig.2c**) to dark green (**Fig.2d**). Furthermore, by employing FT-IR analysis, a new characteristic band for C=N appeared ca. 1654 cm^{-1} as the result of Shiff-base reaction. The continuous decreasing of the transmittance of the finger print band of C=N can well explain the influence of solidification time on the Cu removal performance of CS microspheres (for details, see SI **Fig.S3 and S5b**).

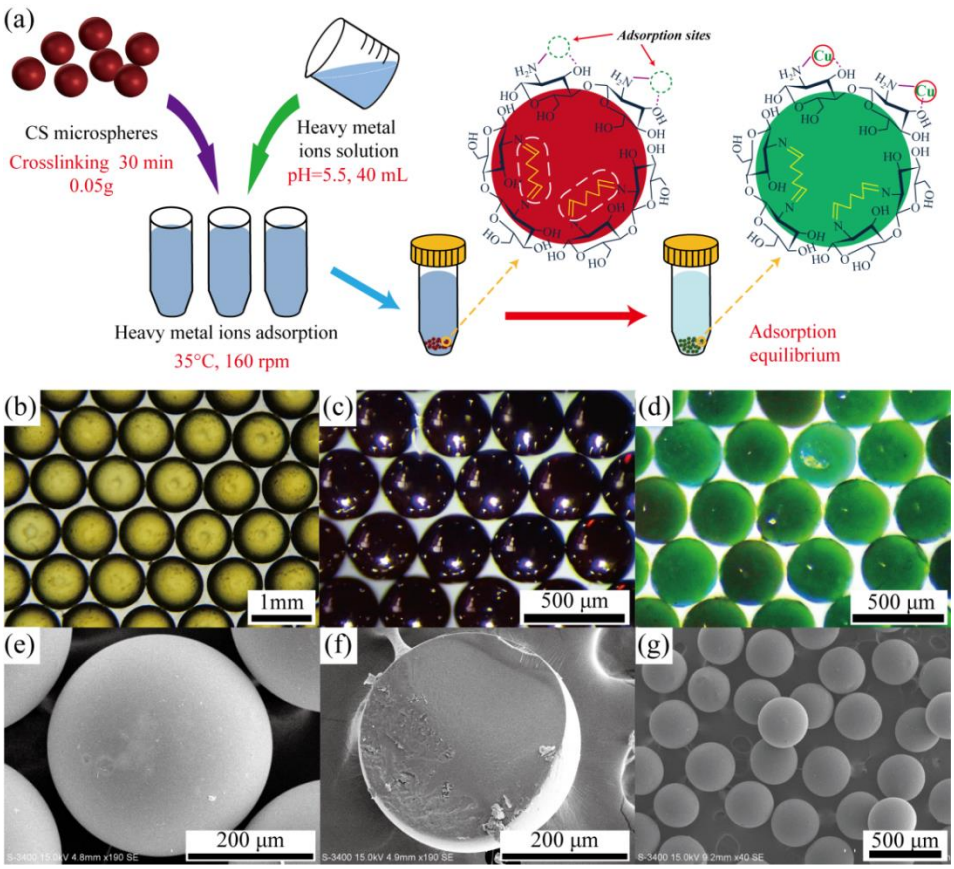

Fig.2. (a) Schematic illustration of batch adsorption experiments; Optical micrograph image of (b) CS emulsion templates with cross-linking time 30 min., (c) before and (d) after adsorption process; The SEM micrographs of (e) the surface and (f) inner structures of single CS microsphere, as well as (g) a certain amount of CS microspheres.

3.2. Adsorption kinetics

Kinetics models are generally introduced to describe the adsorption process and to predict the time needed for adsorption and the rate of target sorbate uptake. To better understand the adsorption behavior of heavy metal ions, herein taking Cu as model ion, the following kinetic models were considered: pseudo-first order model, pseudo-second order model, intraparticle

diffusion model, film diffusion and pore diffusion model. The corresponding kinetics parameters are summarized in **Table 2**.

3.2.1. Pseudo-first order and -second order model

Pseudo-first order kinetics model is described as:

$$\log(q_e - q_t) = \log q_e - \frac{k_1}{2.303} t \quad (3)$$

where q_e (mg g^{-1}) and q_t (mg g^{-1}) are the corresponding amounts of adsorbed Cu ions at equilibrium and at time *t* (min), respectively; k_1(g mg^{-1} min^{-1}) is the rate constant.

In Eq.(3), the adsorbance q_t at each sample time *t* can be obtained with the following equation:

$$q(t_i) = \frac{C_0 V_0 - \sum_1^{i-1} C_i V - C_i[V_0 - (i-1)V]}{m} \quad (4)$$

where C_0 (ppm) and C_i (ppm) are the initial Cu concentration and the concentration at time t_i (min), respectively; V_0 and V represent the initial volume (L) and the sampling volume (L), respectively; *m* is the adsorbent dosage (g).

The pseudo-second order kinetics model is generally expressed as:

$$\frac{t}{q_t} = \frac{1}{k_2 q_e^2} + \frac{t}{q_e} \quad (5)$$

where k_2 (g mg^{-1} min^{-1}) is the rate constant of pseudo-second order adsorption.

Besides, in order to quantitatively compare the applicability of the above 2 kinetic models, the normalized standard deviation Δq_t was included by using the following equation:

$$\Delta\, q_t(\%) = 100 \times \sqrt{\frac{\sum[(q_{t,exp} - q_{t,cal})/q_{t,exp}]^2}{(n-1)}} \quad (6)$$

where $q_{t,exp}$ (mg g^{-1}) and $q_{t,cal}$ (mg g^{-1}) are the experimental and calculated adsorption values at different sample time t (min), respectively; n is the number of sampling points used in the adsorption kinetic curve.

As shown in **Fig.3a,** it took about 100 h to reach adsorption equilibrium and the final adsorption capacity of CS microspheres was 75.52 mg g^{-1} (**Table 1**), which was significantly higher than that reported in literature [18, 22]. The early-time large transfer of Cu ions to the CS adsorbate microspheres observed from the slope of the adsorption kinetic curve can be attributed to a large specific surface area and abundant adsorption sites on their surface, where the adsorption process began. **Table 1** indicates that the structure of CS microspheres has a direct impact on their adsorption kinetics [32]. For example, the CS microspheres with porous structures show faster adsorption rate and shorter time to reach adsorption equilibrium (see **Table 1**). However, the porous nature of the structure shows negative effect on final adsorption capacity of the material. It is found that, the greater the pores existence and distribution, the less adsorption capacity of the single CS microsphere was obtained due to the reduce chitosan content and the decreased adsorption sites on the surface. In this regard, the obvious improvement of the adsorbance of CS microspheres can be achieved by surficial chemical modification. As shown in **Table 1**, the modified CS microspheres with different functional groups exhibited better adsorption ability. However, the complex and multi-step modified process will bring some irreversible damages to CS microspheres, such as the increased compactness, significant nonuniformity and porous structure loss. As a result, the modified CS microspheres exhibit very fast adsorption rate on the surface at the early adsorption stage. Yet, when the surficial adsorption sites are saturated, the

increased structural compactness will create more difficulties for Cu ions diffusion and adsorption inside the modified CS microspheres. Such findings were also supported by the experimental results from our previous paper [25]. In real-life wastewater treatment processes, adsorption equilibrium is not necessarily to be reached. Therefore, the rate and capacity at the early adsorption stage will be of more practical importance. It indicated the potential advantage of our single step microfluidical fabrication strategy.

Table 1. Performance comparison of chitosan-based adsorbents for Cu ions removal.

Entry 1	**CS microspheres based adsorbents**		**Maximum adsorbance (q_m, mg g^{-1})**	**Equilibrium time (t, h)**
1	Cross-linked CS	**This work**	75.52	100
2		CS microspheres [22]	42.08	> 256
3		CS microspheres [21]	~ 30[a]	> 100[a]
4		CS microspheres [18]	31	100
5	Porous structural CS	Porous CS microspheres [18]	32.5	30
6		Imprint CS microspheres [21]	81.45	64
7	Modified CS	CS-poly(acrylic acid) microspheres [18]	61	100
8		CS-tripolyphosphate gel beads [23]	~ 57	> 80
9		CS-heparin polyelectrolyte complex microspheres [24]	~ 44[a]	> 40[a]
10		Polyethylenimine-CS biosorbents [25]	146	~ 64

[a] Read from the figures.

As shown in **Table 2,** the adsorption curves were better fitted with the pseudo-second order model (see **Fig.3c**) with R^2= 0.999, much higher than that of pseudo-first order model (R^2= 0.859,

see **Fig.3b**). What's more, the result of $\Delta\ q_t$, only 4.2%, proved that the adsorbance values of experiment and calculation were very close.

3.2.2. Intraparticle diffusion model

Apart from the above pseudo-first order and pseudo-second order models, more complex and quantitatively mathematical relationships can further better explain the whole adsorption process by incorporating an intraparticle diffusion model. In general, this relationship was presented as an uptake function with the half-power of time ($t^{0.5}$), rather than *t*. The most commonly used intraparticle diffusion equation for biosorption processes was introduced by Weber and Morris [33]:

$$q_t = k_i t^{0.5} + I \quad (7)$$

where k_i is the intraparticle diffusion rate constant (mg g^{-1} $min^{-0.5}$) and the intercept *I* is obtained by linear fitting of the plot of q_t versus $t^{0.5}$, which is in proportion with the boundary layer thickness. A nearly linear variation in the quantity biosorbed with $t^{0.5}$ can be predicted for a large initial fraction of reactions controlled by intraparticle diffusion rates. However, a multi-linear intraparticle diffusion plot (**Fig.3d**) indicates that 3 relatively independent stages with different rate-limiting existed in the biosorption process. The first sharper stage can be attributed to the extraordinary affinity-induced diffusion of Cu ions through the solution to the external surface of CS microspheres or the boundary diffusion layer of the Cu ions. Compared with the first leap stage, in the second stage the increasing trend of the plot slows down showing that the rate of intraparticle diffusion was further limited. Evolving to the final stage, scarce growth of Cu ions uptake was observed as a result of adsorption equilibrium or extremely low Cu ions

concentration left in the solution. These 3 stages suggest that the biosorption process starts by directed surface adsorption and intraparticle diffusion according to the findings of Ofomaja [34].

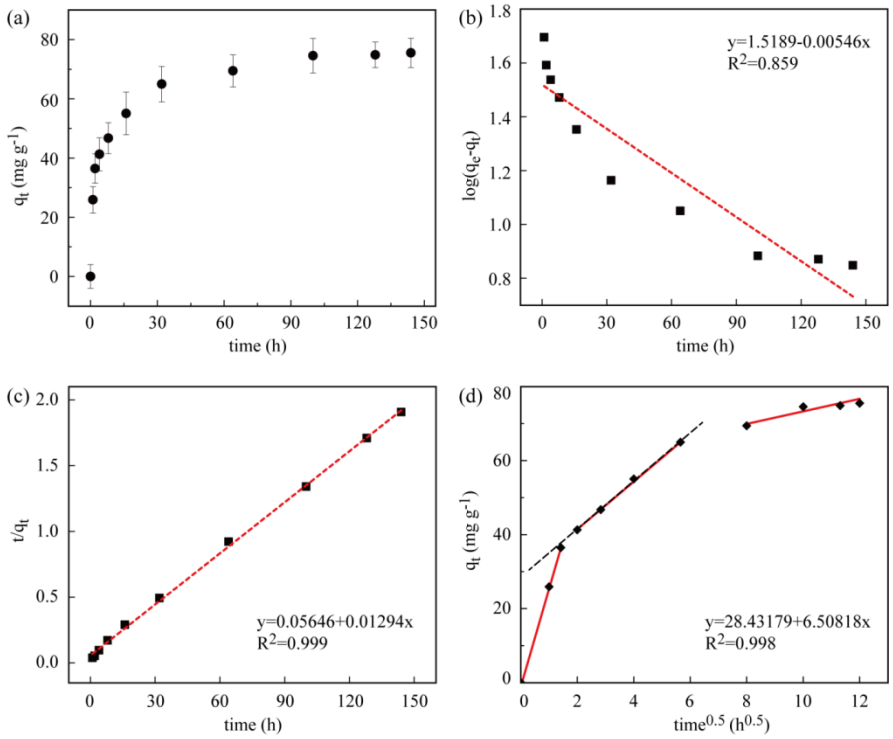

Fig.3. (a) Adsorption kinetics; the linear fitting curve of (b) pseudo-first order model and (c) pseudo-second order model; (d) intraparticle diffusion model.

Table 2. Parameters for adsorption kinetic models at 35 °C, 400 ppm initial Cu concentration (C_0) and 0.05 g CS microspheres load.

Kinetic models	**Parameters**		**Regression coefficient (R^2)**
Pseudo-first order kinetics	$q_{e,cal}$ (mg g^{-1}) 33.029	k_1 (mg g^{-1} min^{-1}) 2.096×10^{-4}	0.859
Pseudo-second order kinetics	$q_{e,cal}$ (mg g^{-1}) 77.280	k_2 (mg g^{-1} min^{-1}) 4.943×10^{-5}	0.999
Intraparticle diffusion	I (mg g^{-1}) 28.432	k_i (mg g^{-1} min$^{-0.5}$) 0.8402	0.998
Film diffusion	D_1 (μm^2 S^{-1}) 0.3866	Intercept 0.3765	0.998

3.2.3. Film diffusion and pore diffusion model

In order to gain more information about the mechanism and rate-controlling steps affecting the adsorption kinetics, film diffusion and pore diffusion were proposed to study the adsorption process. The film diffusion equation can be expressed as

$$\frac{q_t}{q_e} = 6\left(\frac{D_1}{\pi a^2}\right)^{0.5} t^{0.5} + C \quad (8)$$

where a (μm) is the average radius of CS microspheres and D_1 is the film diffusion coefficient ($\mu m^2\ S^{-1}$).

As shown in **Fig.4a**, the plots trend of q_t/q_e versus $t^{0.5}$ for Cu uptake is in conformity with intraparticle diffusion, including 3 sections. The diffusion of Cu ions through the boundary layer from external surface of CS microspheres shows a dominant control.

By comparatively applying the pore diffusion model, we can further describe the adsorption kinetics. Reichenberg expressed the pore diffusion equation [35] as:

$$\text{for } \frac{q_t}{q_e} > 0.85,\ Bt = -0.4977 - \ln\left(1 - \frac{q_t}{q_e}\right) \quad (9a)$$

$$\text{and for } \frac{q_t}{q_e} < 0.85,\ Bt = \left(\sqrt{\pi} - \sqrt{\pi - \left(\frac{\pi^2}{3} \times \frac{q_t}{q_e}\right)}\right)^2 \quad (9b)$$

B can be used to calculate the effective pore diffusion coefficient, D_2 ($\mu m^2\ S^{-1}$), from the following equation [36]:

$$B = \pi^2 \frac{D_2}{a^2} \quad (10)$$

At ideal conditions of linearity (Bt vs. t plot) when passing the fit through the origin, the rate of mass transfer is fully described by pore-diffusion control. If the plot is non-linear or only linear

with intercept varying from zero, it can be concluded that film-diffusion or chemical reaction also controls the adsorption rate. In this regard, as shown in **Fig.4b**, the plots of *Bt vs. t* for Cu ion adsorption did not pass through the origin and showed a non-linear segment at short adsorption times, which further corroborated the above arguments that film-diffusion or chemical reaction controls the rate of adsorption during this period [35]. The plots of pore diffusion and the SEM images of CS microspheres were the reciprocal verification that as-prepared CS microspheres presented a solid spherical structure. At most, some nanopores were distributed along the microspheres but show irrelevant (or uncorrelated) influence on adsorption kinetics.

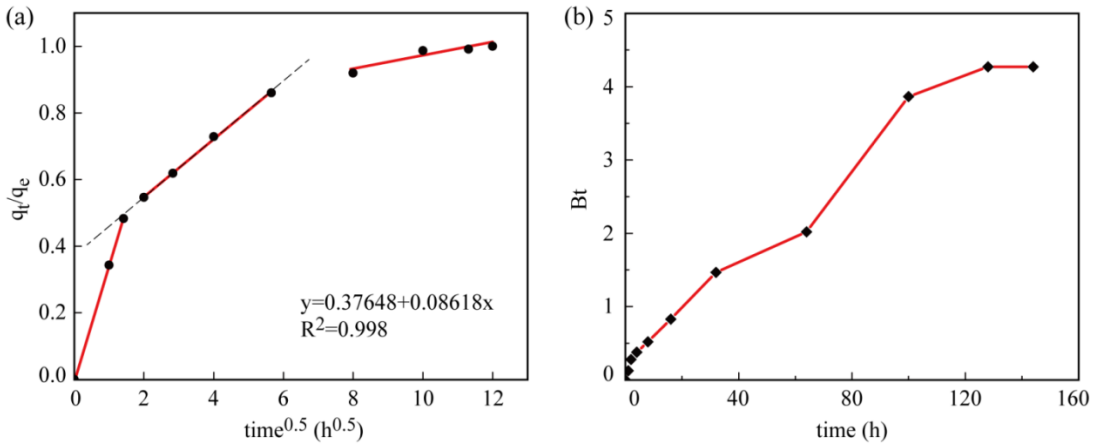

Fig.4. (a) Film diffusion and (b) Pore diffusion model.

3.3. Adsorption isotherms

3.3.1. Langmuir adsorption model

In order to further study the mechanism of Cu ions uptake into the CS microspheres, first the Langmuir adsorption model was adopted to study chitosan-Cu ions interactions as:

$$\frac{C_e}{q_e} = \frac{1}{q_m k_L} + \frac{C_e}{q_m} \qquad (11)$$

where q_m is the maximum adsorption capacity (mg g^{-1}); k_L is the Langmuir constant (L mg^{-1}).

The adsorption isotherm curve was fitted well with Langmuir's equation (Eq.(11)), as show in **Fig.5a**. The calculated maximum adsorption capacity of CS microspheres was 80.32 mg g^{-1}, close to the experiment result. The good fit (R^2= 0.998) in the Langmuir model indicated that the process of Cu ions adsorption can be well described by the assumptions of Langmuir's adsorption model, that is, the adsorbent has uniform and smooth surface, the Cu ions exist at the outer surface of the adsorbent in monolayer and no interaction takes place between the adsorbed Cu ions. Furthermore, the loaded Cu ions will not be replaced at the adsorption sites, which means that the adsorption capacity is determined by the number of adsorption sites [37].

The essential characteristic of the Langmuir isotherm can be further expressed by the separation factor, K_R [38], which is a dimensionless constant and is calculated as the following:

$$\mathrm{K_R} = (1 + \mathrm{k_L C_0})^{-1} \quad (12)$$

where k_L is the Langmuir constant (L mg^{-1}).

K_R values indicate the type of isotherm to be irreversible (K_R=0), favorable (0<K_R <1), linear (K_R=1), or unfavorable (K_R >1). Corresponding to the adsorption of Cu ions onto as-prepared CS microspheres, the calculated K_R values (**Fig.5b**) are in the range of 0.026 - 0.209, indicating that the adsorption is a favorable process.

3.3.2. Freundlich adsorption model

The Freundlich isotherm is an empirical equation usually employed to describe heterogeneous systems. Therefore it is suitable for research in the multi-layer adsorption on the surface of microspheres [39]. The linear form of the Freundlich isotherm model can be represented as:

$$\ln q_e = \ln k_F + \frac{1}{b}\ln C_e \quad (13)$$

where k_F (g mg^{-1}) and b are Freundlich adsorption isotherm constants, being indicative of the extent of the adsorption and the degree of non-linearity between solution concentration and adsorption, respectively.

Although the Freundlich equation agrees well with the Langmuir one over moderate concentration ranges, it does not become the linear isotherm at low surface coverage. Although R^2 of Freundlich adsorption model was still up to 0.916, as shown in **Fig.5c,** it was significantly lower than that of Langmuir one. Therefore, it is concluded that the distribution of the adsorbed Cu ions are in the form of a monolayer on the surface of as-prepared CS microspheres.

3.3.3. Dubinin-Radushkevich (D-R) isotherm model

The Dubinin-Radushkevich (D-R) isotherm model was also fitted to the equilibrium data in order to determine the physical or chemical nature of the adsorption process. This model can be expressed as:

$$\ln q_e = -\beta\varepsilon^2 + \ln q_m \quad (14a)$$

$$\varepsilon = RT\ln(1 + 1/C_e) \quad (14b)$$

where β is the activity coefficient related to adsorption mean free energy ($mol^2\ J^{-2}$); ε is the Polanyi potential; R is the gas constant (8.314 J $mol^{-1}\ K^{-1}$); T is the absolute temperature (K).

The mean free energy of adsorption E (kJ mol^{-1}) can be calculated to estimate the type of sorption process using the following equation [40]:

$$E = 1/\sqrt{2\beta} \quad (15)$$

If E exceeds 8 kJ mol^{-1}, chemisorption becomes the dominant process. Beneath this value, only physisorption is dominant as a result of weak forces between the adsorbate and adsorbent such as Van der Waals forces, rather than chemisorption or ion exchange [41]. The D-R isotherm plot is shown in **Fig.5d**. The calculated value of E was 11.455 kJ mol^{-1} confirms that the Cu ions removal by CS microspheres was a chemisorption process. A general consensus has been made by comparing the results among Langmuir, Freundlich, D-R isotherm model and experimental data for the Cu ions adsorption of CS microspheres, as shown in **Table 3**.

Table 3. Parameters for adsorption isotherm models.

Adsorption isotherms	**Parameters**		**Regression coefficient (R^2)**
Langmuir	q_m (mg g^{-1}) 80.321	k_L (L mg^{-1}) 7.566×10^{-2}	0.998
Freundlich	b 2.555	k_F (g mg^{-1}) 11.20	0.916
Dubinin-Radushkevich	q_m (mol g^{-1}) 3.106×10^{-3}	β ($mol^2\ kJ^{-2}$) 3.810×10^{-9}	0.960

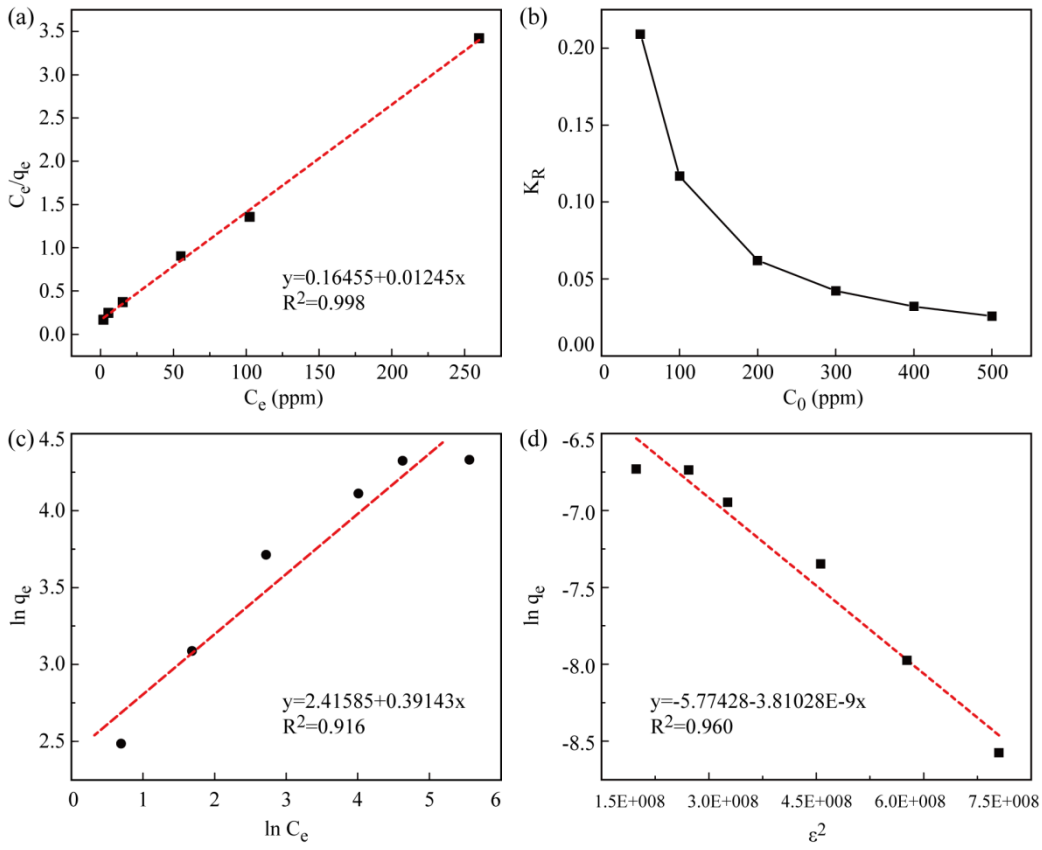

Fig.5. (a) Langmuir adsorption isotherm; (b) the separation factor for Cu ions adsorption; (c) Freundlich adsorption isotherm; and (d) D-R adsorption isotherm of CS microspheres.

3.4. Adsorption mechanism

Based on the SEM images (**Fig.6a-c**) of the CS microspheres, recovered from adsorption experiments with varying contact time (16, 32 and 100 h), an obvious morphological change was observed as a result of the Cu accumulated process. In detail, the amount of attachments observed on the surface of CS microspheres increases with longer contact time. The initial smooth surface became gradually more rough when reaching adsorption equilibrium. Besides, the attachments uniformly covered CS microspheres, which are in accordance with the results of Langmuir model and further demonstrate that the existing state of Cu ions on the surface of CS microspheres exist in monolayers without interaction. Moreover, the elements distribution of Cu

on the surface and interior (cross-section) of CS microspheres with different adsorption time were visualized using EDX analysis. **Fig.6d-f** show the sequential change of Cu distribution on the surface of the CS adsorbent, consistent with the SEM images (**Fig.6a-c**). Additionally, the changing trend of the Cu distribution inside (**Fig.6g-i**) showed a similarity with that on the surface, but displayed some delay in time with the surface, which can be attributed to internal diffusion resistance. It further supports the non-linear relationships obtained in intraparticle, film and pore diffusion, as presented in **Fig.3d, 4a** and **4b**, respectively. At the same time, the initial Cu distribution change (from **Fig.6d** to **Fig.6e**) was more obvious than that when close to the adsorption equilibrium (from **Fig.6e** to **Fig.6f**). More importantly, the Cu distribution decreased progressively when moving from the surface to the interior of CS microspheres. There is almost no Cu element response in the center of the CS microsphere at the first adsorption stage (**Fig.6g**), as a result of the direct affinity of the active surface amino groups and the greater internal diffusion resistance.

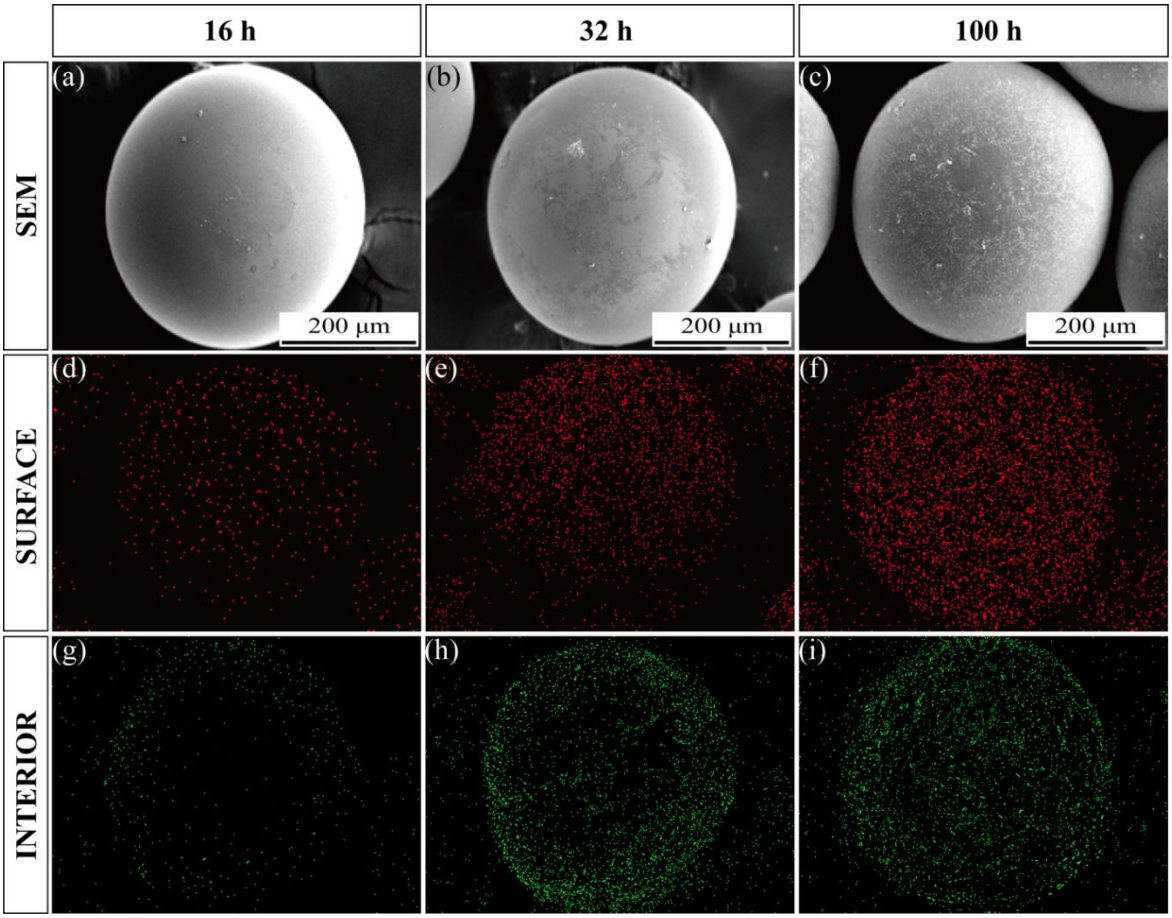

Fig.6. (a-c) SEM images of the surface of CS microspheres with increasing Cu ion contact time; EDX images of the (d-f) surface and (g-i) interior of CS microspheres with increasing Cu ion contact time.

Based on the theoretical modeling analysis and EDX observation, the adsorption process was described schematically (**Fig.7**). As shown in **Fig.7a**, the parent cross-linked CS microspheres provide a large amount of adsorption sites not only on the surface but also inside. The intraparticle diffusion (**Fig.7b**) controls the first contact process between as-prepared CS microspheres and the Cu ions solution. Subsequently, Cu ions penetrate the boundary layer and reach the surface of CS microspheres depending on the film diffusion resistance (**Fig.7c**). Active amino groups on the surface of CS microspheres with strong affinities towards Cu ions gave rise to fast Cu uptake (**Fig.7d**). At this stage, surface mediated chemisorption is predominant.

Simultaneously, a growing number of Cu ions migrate inside but show a substantial adsorption delay due to internal diffusion resistance limitations (**Fig.7e**). Although no clear porous structure was observed in the SEM images, the tiny pores still play an assistant role in the flux of Cu ions from the exterior to the interior of CS microspheres. In addition, once the adsorption sites were occupied, they could not be occupied again. When both the surface and internal adsorption sites were saturated, the apparent adsorption equilibrium was reached (**Fig.7f**). However, the whole adsorption process is limited and affected by several factors, such as cross-linking degree, aqueous solution pH, and so on. This trade-off between adsorption capacity and stability will be discussed in the SI **Fig.S5**.

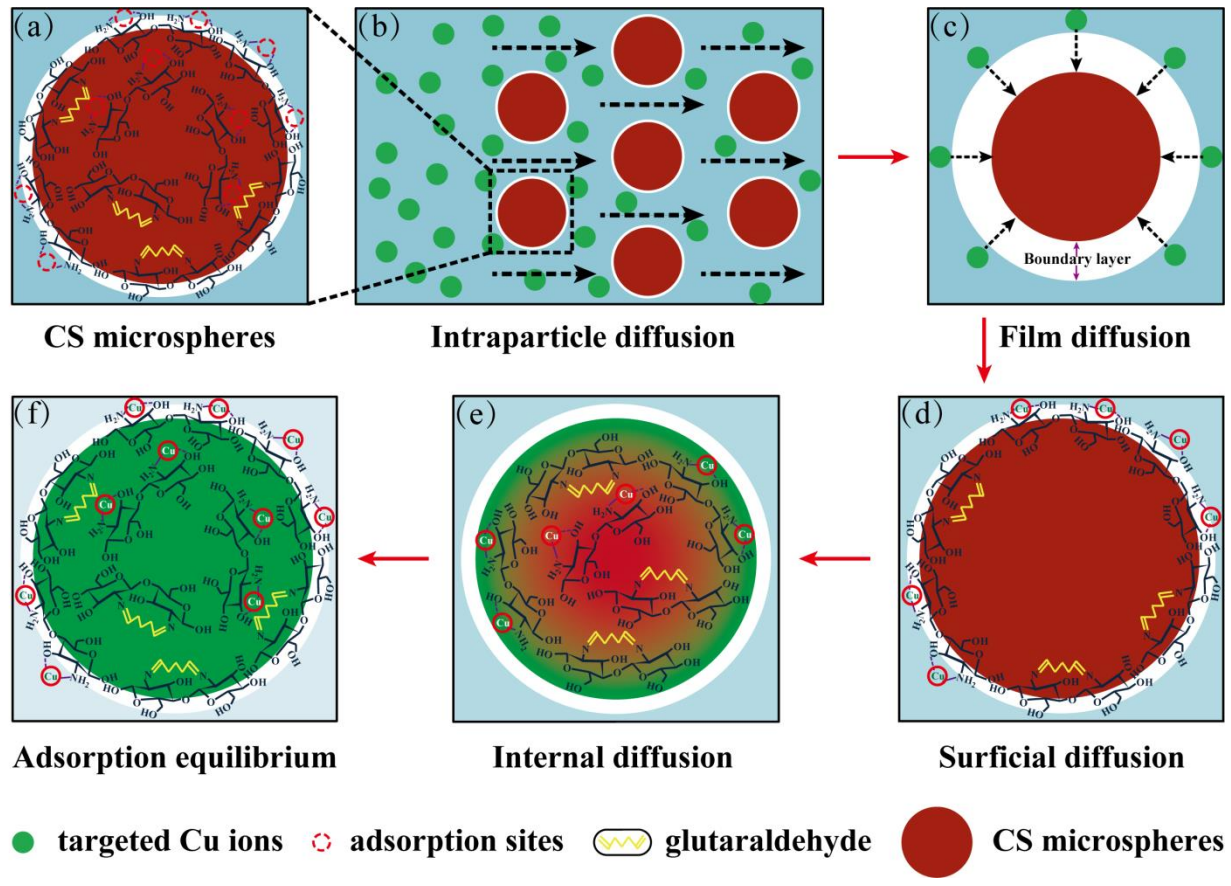

Fig.7. Schematic illustration of the adsorption mechanism.

3.5. High selectivity toward targeted ions

In real life contaminated waters, other components co-exist with the target adsorbate, sometimes in complex media, which lead to adsorbent poisoning. Therefore, it is necessary to investigate the selectivity of CS microspheres towards targeted ions for further practical applications.

Next to Cu, Na and Al ions, which are widely abundant in many water sources, were added in the adsorption experiments to study the selective removal of Cu ions by CS microspheres. Different aqueous solutions were prepared (e.g. 400 ppm Cu^{2+} with 400 ppm Na^{+} and/or Al^{3+}; and 100 ppm Cu^{2+} with 400 ppm Na^{+} and/or Al^{3+}). The results are displayed in **Fig.8a**, showing that as-prepared CS microspheres were selective towards Cu ions in all cases. At identical metal concentrations (400 ppm), the selectivity towards Cu ions can reach up to 86.78%. The adsorption capacities of Na and Al ions were quite small, only 4.53% and 8.69%, respectively. At more realistic conditions (100 ppm Cu and 400 ppm Na and Al), CS microspheres still presented stronger adsorption ability towards Cu ions (83.1%) than the other two ions (5.82% for Na and 11.08% for Al ions, respectively). More details can be found in SI, **Fig.S7a**.

Besides, the adsorbance and selectivity of as-prepared CS microspheres in another more complex aqueous solution containing several toxic metal ions, such as Co and Mn, with the same valence state as Cu, were also deeply studied. Similarly, several aqueous solutions were prepared as above (e.g. 400 ppm Cu^{2+} with 400 ppm Co^{2+} and/or Mn^{2+}; and 100 ppm Cu^{2+} with 400 ppm Co^{2+} and/or Mn^{2+}). The experimental results (**Fig.8b**) indicated that although Co and Mn ions have a greater influence on the selective adsorption of as-prepared CS microspheres towards targeted Cu ions, the maximum adsorbance of these two metal ions (15.81% for Co and 11.78% for Mn ions) could not surpass that of Cu ions (72.41%). The consistent conclusion of selective

adsorption for targeted Cu ions has been demonstrated under more extreme conditions (100 ppm Cu^{2+} with 400 ppm Co^{2+} and/or Mn^{2+}) (See SI, **Fig.S7b**).

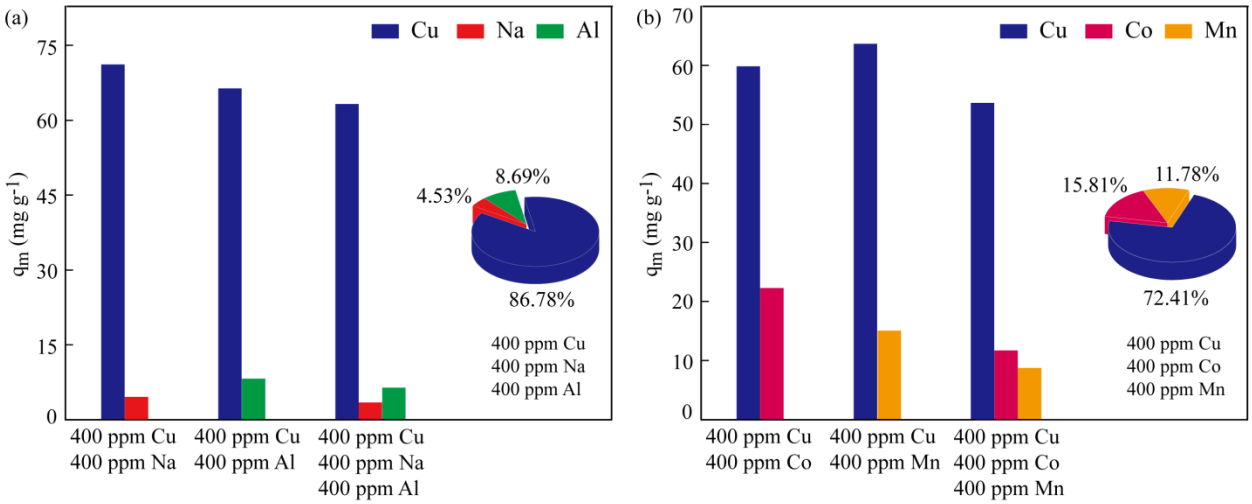

Fig.8. The adsorption selectivity towards Cu ions (as histograms) and the adsorption rate of Cu ions (as charts) in contaminated water in the presence of other competitive metal ions: (a) Na and Al ions; (b) Co and Mn ions.

3.6. Selective binding mechanism

3.6.1. Ionic scale effect and electronegativity

In order to investigate the selective adsorption mechanism of CS microspheres towards Cu ions, ionic scale effect was firstly introduced. Since the long straight chain of chitosan molecule turned into intricate spatial network structure during the Schiff-based reaction, therefore, the ionic size will show an undoubted impact on the adsorption properties of CS microspheres. The radii of investigated metal ions were listed and compared in **Table 4**.

Table 4. The comparison of different metal ionic radii (Unit: nm).

Na^{+}	Co^{2+}	Cu^{2+}	Mn^{2+}	Al^{3+}
0.102	0.0745	0.073	0.067	0.0535

As shown in **Table 4**, the radii of investigated metal ions followed the order that $Na^{+} > Co^{2+} \approx Cu^{2+} > Mn^{2+} > Al^{3+}$. The experimental results demonstrated that as-prepared CS microspheres show better adsorption capacity towards bivalent metal ions than Na and Al ions. This phenomenon can be explained as suitable ion size is beneficial for adsorption, conversely, oversize or undersize ions will hinder the coordinate binding between metal ions and active adsorption sites of CS microspheres. As shown in **Fig.8a**, the adsorbed Na ions on CS microspheres may be the result of the inefficient physisorption process, such as intraparticle diffusion. By contrast, in consideration of the charge number of Al ions is greater than Cu ions, thus, in theory, more binding sites (either amino or hydroxyl groups) will be consumed by adsorbing Al ions than Cu ions under the same number of adsorption sites. Thus, the poor adsorption performance towards Al ions, which is attributed to the synergistic action of ionic scale and charge effect, can be predictable.

Besides, electronegativity (χ), which is the inherent character of an element, represents the relative attraction of an atom for the valence electrons in a covalent bond. It is directly proportional to the effective nuclear charge but inversely proportional to the covalent radius, which can be expressed as follow:

$$\chi = \frac{0.31(n+1\pm c)}{r} + 0.50 \quad (16)$$

where *n* is the number of valence electrons, *c* is any formal valence charge on the atom, and *r* is the covalent radius.

The electronegativity values of the targeted metal elements in this study can be found in Lange's handbook [42], showing in **Table 5**. Because of the fact that higher electronegativity of a metal

ion represents higher attraction of metal ion for electrons [43], thus, Cu ions show an incomparable strong affinity to CS microspheres.

Table 5. Electronegativity values of the targeted elements.

Na	Mn	Co	Cu	Al
0.93	1.55	1.88	1.90	1.61

Electronegativity order: Cu > Co > Al > Mn > Na

3.6.2. Density functional analysis

3.6.2.1 Adsorption energy (Δ*E*)

Density functional theory (DFT) has recently been widely recognized as an efficient quantum chemistry method for studying molecular properties and a powerful tool to predict the geometries and calculate the binding energies of metal-chitosan complexes [44-47]. Thus, for further explanation of selective adsorption mechanism, adsorption energy (Δ*E*) has been quantitatively compared by using DFT analysis in the more favorable binding models (**Fig.9**), that is, *pendant model*, *bridge model* and *central model*, respectively [45]. For more details on DFT calculation simplification and structural optimization of metal complexes, see SI.

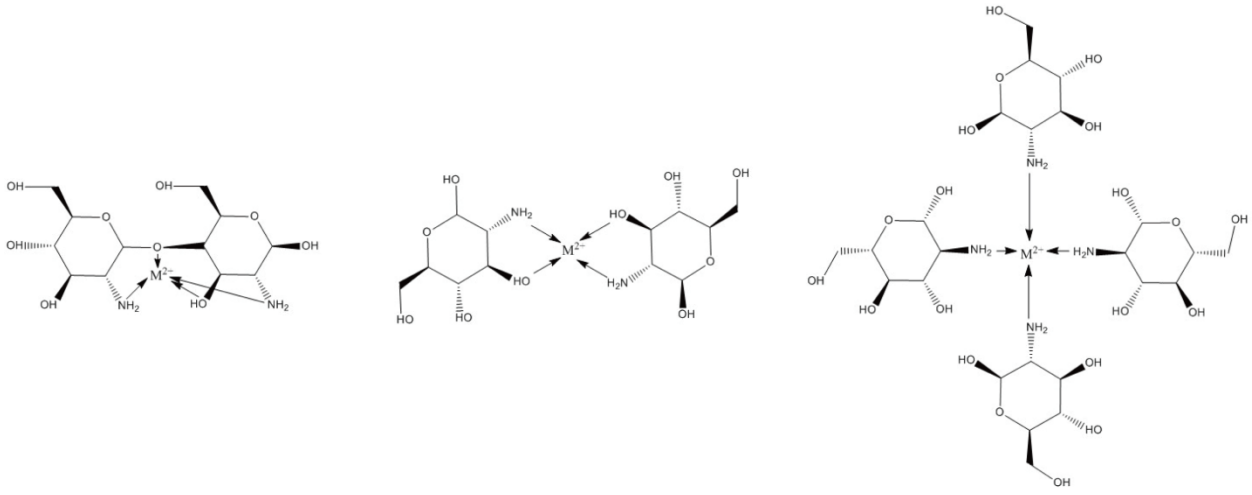

Pendant model **Bridge model** **Central model**

Fig.9. Structures of investigated metal-CS complexes. Water molecules are not shown for the simplicity reason. ($[M]^{2+}$ was used to represent the divalent metal ions, including Cu^{2+}, Co^{2+} and Mn^{2+}.).

The energies of different components and the corresponding adsorption energies (ΔE) of metal-CS complexes in three optimized models were listed and compared in **Table 6**. Besides, the representative 3D structures of Cu-CS complexes with optimized geometries are shown in **Fig.10**. 3D structures for all calculated metal complexes are shown in **Fig.S8** and **Fig.S9** (See SI).

Table 6. The energies (E) and adsorption energy (ΔE) of different metal complexes.

Ions	Models	Energies (E) (kJ mol^{-1})			Adsorption energy (ΔE) (kJ mol^{-1})
		Ions	CS microspheres	Complexes	
Cu	Pendant model	-513,573	-3,304,473	-3,818,670	-624
	Bridge model		-3,505,237	-4,019,518	-708
	Central model		-7,010,585	-7,524,908	-750
Co	Pendant model	-379,804	-3,304,473	-3,684,667	-390
	Bridge model		-3,505,237	-3,885,517	-476
	Central model		-7,010,585	-7,390,912	-523
Mn	Pendant model	-271,723	-3,304,473	-3,576,611	-415
	Bridge model		-3,505,237	-3,777,428	-468
	Central model		-7,010,585	-7,282,784	-476

Selective adsorption order: Cu > Co > Mn

The DFT calculation results (**Table 6**) are consistent with the experimental conclusions (**Fig.8** and **Fig.S7**) as well as the previous literature [48], which provide a reliable theoretical basis for selective adsorption of as-prepared CS microspheres for Cu ions. As shown in **Table 6**, the results of ΔE showed that the selective adsorption performance of as-prepared CS microspheres is in the order: Cu > Co > Mn. Although the ΔE values of the same metal complex varied significantly in different models, CS microspheres always showed the strongest binding energy towards Cu ions in all three models. Besides, it was also demonstrated that the most energetically

favorable structure of the investigated metal complexes was *central model*, since the obtained ΔE value was larger than those of the other two binding models. In other words, metal ions prefer to form metal chelates as *central model* through the coordinate binding with multiple amino groups, rather than with the amino and hydroxyl groups simultaneously. This conclusion is in accordance with previous article [46], that is, metal ions binding with the nitrogen atom of amino group is stronger than that with oxygen atom of hydroxyl group from either chitosan monomer or water molecule. Furthermore, it also verified that the adopted simplified DFT calculation, which excludes the effect of interaction between metal ions and water molecule, is feasible.

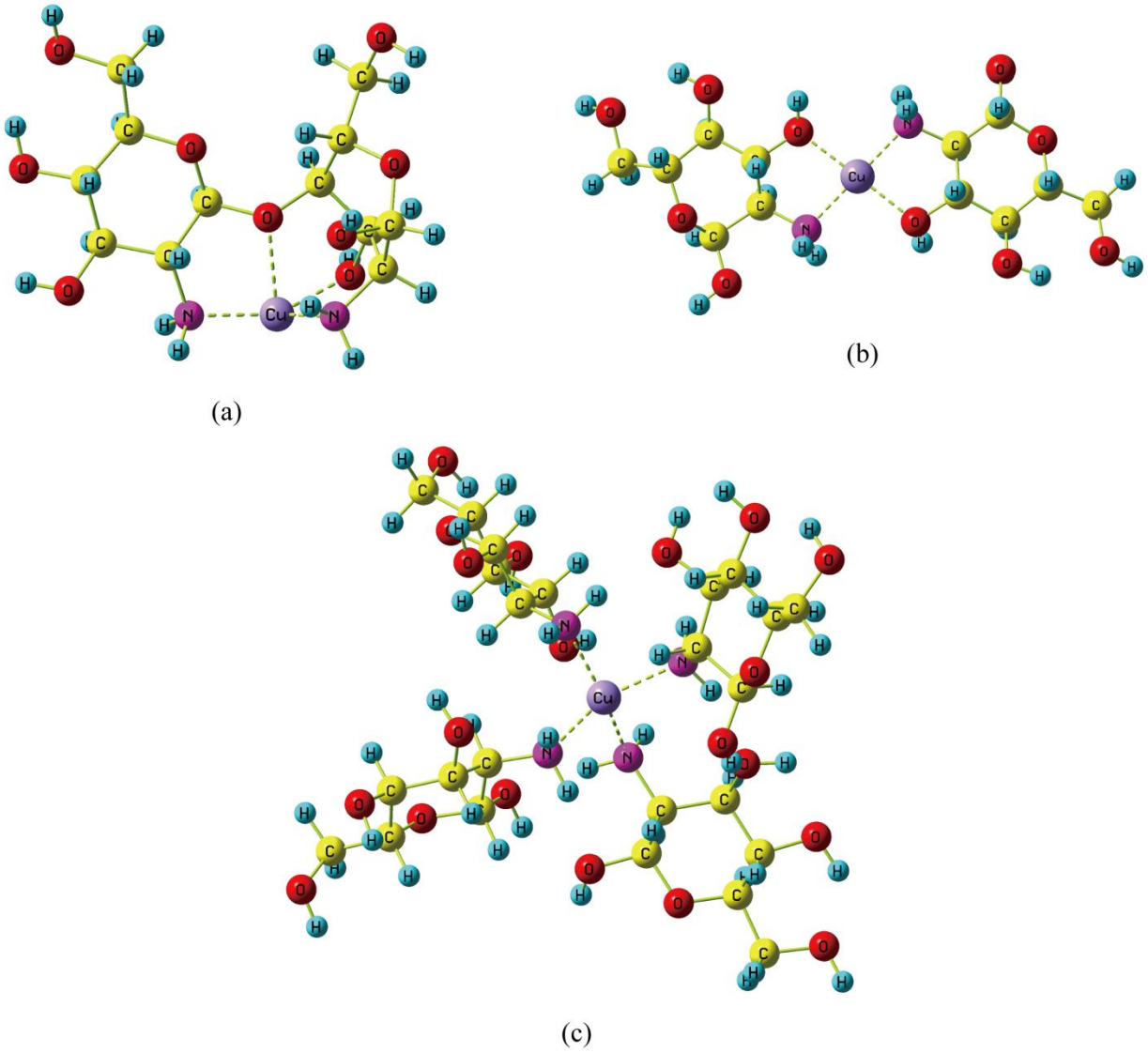

Fig.10. Representative 3D-models of geometrically optimized Cu-CS complexes for (a) pendant model, (b) bridge model and (c) central model.

3.6.2.2 Frontier molecular orbitals

In order to gain more insight into how the chitosan monomer interaction at the molecular with metal ions, frontier molecular orbitals and natural bond orbitals were subsequently analyzed. The

highest occupied molecular orbitals (HOMOs) and the lowest-lying unoccupied molecular orbitals (LUMOs) are known as frontier molecular orbitals (FMOs), which play a vital role in determining molecular properties and elucidating information regarding charge transfer within the molecule [49]. The HOMO represents the ability to donate an electron, while LUMO as an electron acceptor represents the ability to capture an electron. The difference between LUMO and HOMO (E_L-E_H), known as energy gap ($\Delta E'$, kJ mol^{-1}), is regarded as an important parameter to predict the reactivity, stability of complexes formed and also the conductance of molecules [46, 50].

For the purpose of deeply revealing the binding mechanism of metal ions and chitosan monomers, the selective adsorption procedure can be further simplified as the coordinate binding process between a metal ion and a chitosan monomer. In this work, the frontier molecular orbitals and molecular electrostatic potential were computed using DFT(B3LYP) method with 6-31+G(d,p) basis sets. The HOMO-LUMO energy differences of chitosan monomer and metal complexes are presented in **Table 7**.

Table 7. Calculated energies of chitosan monomer and metal complexes.

	E_L	E_H	$\Delta E'$ (kJ mol^{-1})	$\Delta E'$ (eV)
Chitosan monomer	-0.00322	-0.25063	649.575	6.75558
Cu complex	-0.10828	-0.30527	517.1972	5.37885
Co complex	-0.18426	-0.29609	293.6097	3.05354
Mn complex	-0.11839	-0.29049	451.8486	4.69923

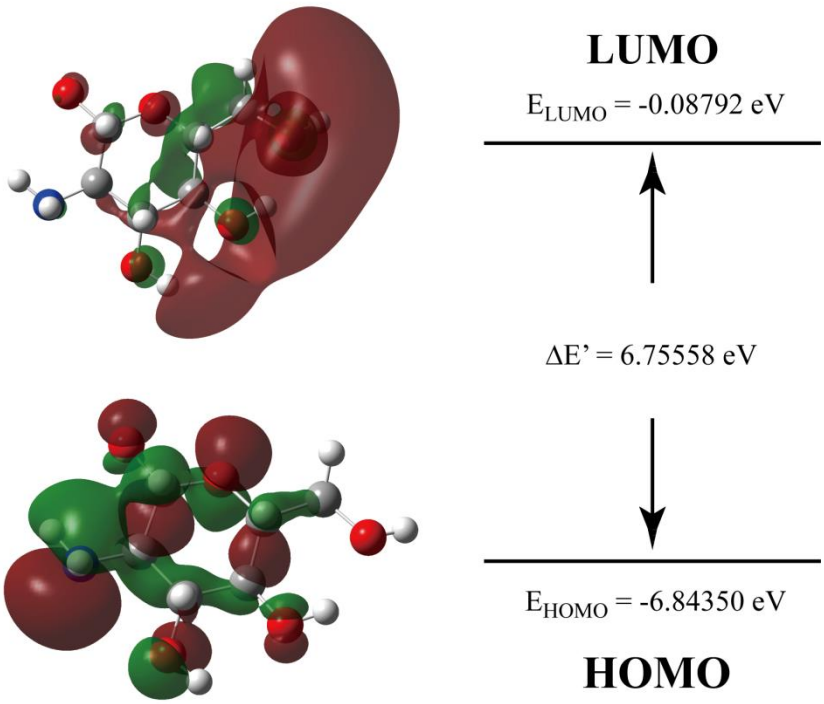

Fig.11. Molecular orbital surfaces and energy levels for HOMO and LUMO of chitosan monomer.

As seen from **Fig.11**, the HOMO orbitals were mainly localized on the amino group, neighboring hydroxyl groups as well as the six-membered aromatic ring, while LUMOs are distributed on the far end of the chitosan monomer molecule and opposite to the amino position. After the formation of metal complex with the optimized configuration (see **Table 7**), the values show that the energy difference ($\Delta E'$) of Cu complex is larger than the other two metal complexes, which indicates that Cu complex is most stable, following the principle that the stability of complexes increases with increase in energy gap [43]. Besides, the $\Delta E'$ value, which given in electron volt in **Table 7**, can also be used for the conductance studies. The conductance of metal complex follows the reverse order. It can be explained that the positive charge on metal ion is redistributed under complexation. Among the three metal ions, Cu ion carries lowest positive charge in the Cu complex, and thus its corresponding

conductance is lowest. Additionally, in the coordinational binding process between metal ion and chitosan monomer, the electrons in the outer orbital of Cu ion have been proved to present higher transition energy, which is beneficial for the electron transition in energy level orbits and the preferential combination between the free electron and electron hole.

The molecular electrostatic potential (MEP) is related to the electronic density and is a very useful descriptor for predicting reactive sites for electrophilic and nucleophilic attack as well as hydrogen-bonding interactions [49, 51]. Herein, MEP was calculated at the B3LYP/6-31+G(d,p) method at the 0.02 isovalues and 0.0001 density values. The negative electrostatic potential portion of the investigated molecule is susceptible to electrophilic attack. In other words, the degree of electrophilic attack will increase with the increase of the negative electrostatic property. The color scheme for the MEP surface (see **Fig.12**) is as follows: red for electron-rich region with strong negative charge; blue for electron-deficient region with strong positive charge; green for neutral; respectively. Consequently, electrostatic potential increases in the order: red < green < blue. The color code of this map, where the negative (red and yellow) regions are related to electrophilic reactivity while the positive (blue) ones to nucleophilic reactivity, is in the range between -2.299 eV (deepest red) to 2.299 eV (deepest blue) in the chitosan monomer molecule.

As can be seen in **Fig.12**, the region defined by amino group and adjacent hydroxyl group in the chitosan monomer molecule exhibits the strongest electrophilic property. Besides, the N atom in amino group and O atom in neighboring hydroxyl group present the highest negative V(r) values, -0.049 a. u. and -0.031 a. u., respectively. All of these indicate that this region is the most possible and preferable site for metal ions binding. Oppositely, the maximum positive region (blue color) is mainly localized around the oxygen atom in the hydroxyl group on the other side of chitosan monomer molecule with a value of 0.034 a. u.

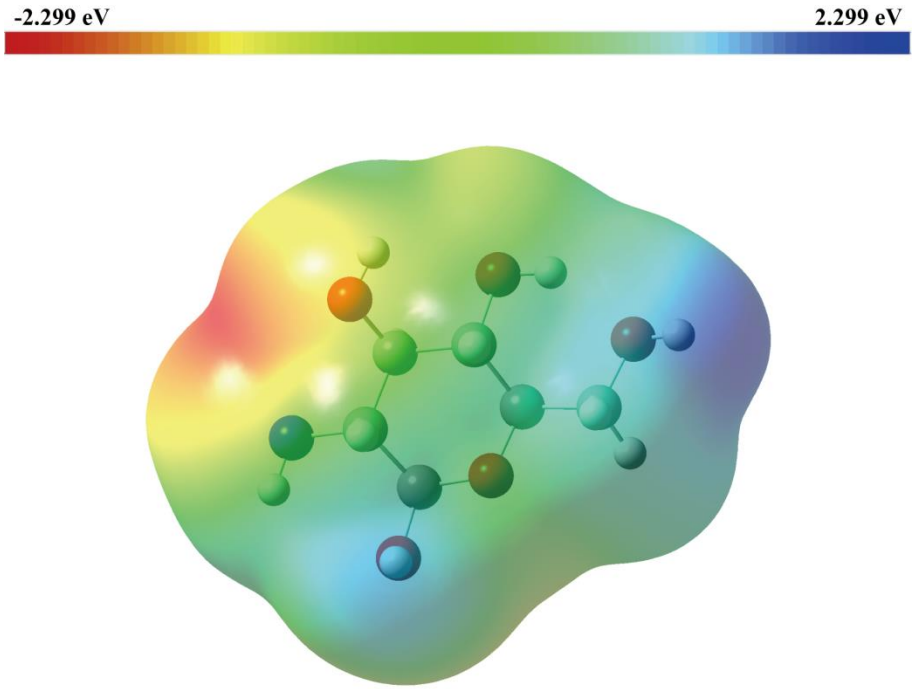

Fig.12. Molecular electrostatic potential map calculated at B3LYP/6-31+G(d,p) level.

3.6.2.3 Natural bond orbitals

The electron configurations of the metal ions as well as the natural charge of the metal atoms in complexes were calculated using the natural population analysis method (NPA) and the results are summarized in **Table 8**. The change of the natural charge of the targeted metals is closely related to the natural population of the metal ions on the *3d* orbit [52]. Although the metal ion *3d* population increases significantly from Mn(II) to Cu(II) (5.14-9.49), the *4s* (0.06-0.13) and *4p* (0.02) population remain basically unchanged in all complexes. This trend indicates that the *3d* orbital participation in the coordination bond is the dominant factor of the charge variation on the metal ions. As the *3d* population of the metal ions increased, the trend of charge transfer from amino and hydroxyl group to the metal ions increased, resulting in metal ions retaining less positive natural charge in the corresponding complexes [52-54]. As seen (**Table 8**), the total

amount of charge transfer from function group of chitosan monomer to the metal ion decreases as the following order: Cu > Co > Mn. In addition, as expected, the covalent bonding of metal ions with amino group in chitosan monomers has a higher priority. The calculated NPA results can well explain the selective adsorption performance of as-prepared CS microspheres that the *3d* orbital population of metal ions plays a significant role in the valence shell of the complexes, resulting in preferential binding of Cu ions towards chitosan monomer.

Table 8. Summary of the electronic configuration of the metal ions and charge distribution of the metal complexes calculated by natural population analysis (NPA).

	Charge distribution			**Metal configuration**
	N	**O**	**Metal**	
Cu	-0.62	-0.559	0.96	$4s^{0.13}\,3d^{9.49}\,4p^{0.02}$
Co	-0.577	-0.551	1.174	$4s^{0.08}\,3d^{7.38}\,4p^{0.02}$
Mn	-0.771	-0.635	1.499	$4s^{0.06}\,3d^{5.14}\,4p^{0.02}$

Selective adsorption order: Cu > Co > Mn

3.7. Desorption and regeneration

The re-usability of adsorbents is critical for industrial applications. Especially, the fast desorption from the adsorbents with minimal damage is highly demanded. In our study, a 0.5 M NaOH solution containing 1.5 wt% EDTA was used as the desorption solution to test the re-usability of the recovered CS microspheres and achieve fast desorption process in terms of seconds. The desorption procedure without EDTA involvement was also studied for desorption efficiency comparison (See SI). The $q_{r,m}$ and R_E values in different adsorption-desorption cycles are displayed in **Fig.13a** and **b**, respectively. Although the re-adsorption capacity ($q_{r,m}$) and efficiency (R_E) of CS microspheres decreased almost inevitably, they exhibited acceptable

regeneration as R_E was still higher than 74% after 5 adsorption-desorption circles. Besides, after the desorption process, the colorless and transparent desorption solution turned light blue and CS microspheres turned back into reddish brown as shown in **Fig.13c**, which indicated that the loaded Cu ions were desorbed in substantial amounts. Furthermore, these microspheres turned into dark green again in the re-adsorption process and the final color of Cu ions solution turned almost colorless (**Fig.13d**). These evidences demonstrated illustrate the good re-utilization capacity of the as-prepared CS microspheres. However, there is still room for further improvement of their re-adsorption performance.

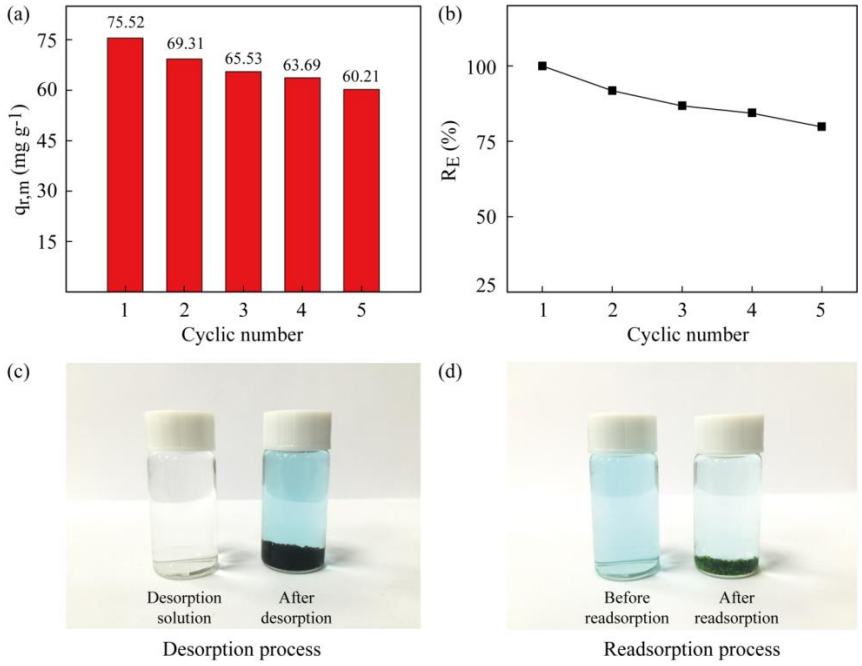

Fig.13. (a) Maximum re-adsorption capacity ($q_{r,m}$) and (b) re-adsorption efficiency (R_E) of CS microspheres during 5 adsorption-desorption cycles; Photographs of the color change of (c) desorption solution and (d) Cu ions solution before and after re-adsorption.

4. Conclusion

A set of novel CS microspheres with outstanding characteristics, such as high monodispersity and controllable size, were successfully synthesized using a facile one-step microfluidic technology. More importantly, not only the enhanced adsorption capacity, distinguished selectivity and re-usability towards Cu ions of the as-prepared CS microspheres were confirmed and measured by batch adsorption experiments, but also the multi-step adsorption process was unprecedentedly revealed by our adsorption mechanism analytic system in the form of quantitative measurements and schematic description. The excellent adsorption performance together with the biodegradable feature and relatively low production cost make that microfluidically-synthesized CS microspheres area promising material for the removal of Cu ions and potentially of other toxic heavy metal ions from contaminated water in the industrial wastewater treatment applications. Especially, it is proven by DFT analysis that the superior selective removal characteristics of CS microspheres in the present of other competitive ions with different valence states can be attributed to both ionic scale effect, inherent high electronegativity and strong adsorption energies (ΔE). Moreover, the integrated adsorption mechanism analytic system provides a practical guidance to evaluate the performance of novel adsorbent materials and to reveal the adsorption mechanism in depth, hereby improving the control of wastewater pollutants in the future.

Acknowledgements

This work is supported by The National Basic Research Program of China (973 Program, 2014CB748500), National Natural Science Foundation of China (51406057, 51578239, 51322805) and Research Fund for the Doctoral Program of Higher Education of China (20130074120019).

Appendix A. Supplementary data

Supplementary data associated with this article can be found in SI.

References

[1] R. Martinez-Palou, R. Luque, Applications of ionic liquids in the removal of contaminants from refinery feedstocks: an industrial perspective, Energy & Environmental Science, 7 (2014) 2414-2447.

[2] S. Mahiya, G. Lofrano, S. Sharma, Heavy metals in water, their adverse health effects and biosorptive removal: A review, International Journal of Chemistry, 3 (2014) 132-149.

[3] H.Y. Lee, D.R. Bae, J.C. Park, H. Song, W.S. Han, J.H. Jung, A Selective Fluoroionophore Based on BODIPY-functionalized Magnetic Silica Nanoparticles: Removal of Pb2+ from Human Blood, Angewandte Chemie International Edition, 48 (2009) 1239-1243.

[4] Y. Guo, H. Guo, Y. Wang, L. Liu, W. Chen, Designed hierarchical MnO2 microspheres assembled from nanofilms for removal of heavy metal ions, RSC Advances, 4 (2014) 14048-14054.

[5] X. Wang, X. Ma, Z. Yang, Z. Zhang, J. Wen, Z. Geng, Z. Wang, An NBD-armed tetraaza macrocyclic lysosomal-targeted fluorescent probe for imaging copper(ii) ions, Chemical Communications, 49 (2013) 11263-11265.

[6] M. Vafaeezadeh, M.M. Hashemi, N. Ghavidel, Polarity adjustment of a nanosilica-functionalized polyamine modified by ionic liquid for removal of Cu2+ from aqueous solutions, RSC Advances, 6 (2016) 14128-14133.

[7] C.d.G. Sampaio, L.S. Frota, H.S. Magalhães, L.M.U. Dutra, D.C. Queiroz, R.S. Araújo, H. Becker, J.R.R. de Souza, N.M.P.S. Ricardo, M.T.S. Trevisan, Chitosan/mangiferin particles for

Cr(VI) reduction and removal, International Journal of Biological Macromolecules, 78 (2015) 273-279.

[8] F. Fu, R. Chen, Y. Xiong, Application of a novel strategy—Coordination polymerization precipitation to the treatment of Cu2+-containing wastewaters, Separation and Purification Technology, 52 (2006) 388-393.

[9] Z. Wang, Y. Feng, X. Hao, W. Huang, X. Feng, A novel potential-responsive ion exchange film system for heavy metal removal, Journal of Materials Chemistry A, 2 (2014) 10263-10272.

[10] F. Akbal, S. Camcı, Copper, chromium and nickel removal from metal plating wastewater by electrocoagulation, Desalination, 269 (2011) 214-222.

[11] S.F. Alshahateet, A.G. Jiries, S.A. Al-Trawneh, A.S. Eldouhaibi, M.M. Al-Mahadeen, Kinetic, equilibrium and selectivity studies of heavy metal ions (Pb(II), Co(II), Cu(II), Mn(II), and Zn(II)) removal from water using synthesized C-4-methoxyphenylcalix[4]resorcinarene adsorbent, Desalination and Water Treatment, 57 (2016) 4512-4522.

[12] R. Li, L. Zhang, P. Wang, Rational design of nanomaterials for water treatment, Nanoscale, 7 (2015) 17167-17194.

[13] M.M. Khin, A.S. Nair, V.J. Babu, R. Murugan, S. Ramakrishna, A review on nanomaterials for environmental remediation, Energy & Environmental Science, 5 (2012) 8075-8109.

[14] M. Rinaudo, Chitin and chitosan: Properties and applications, Progress in Polymer Science, 31 (2006) 603-632.

[15] C. Shen, Y. Wang, J. Xu, G. Luo, Chitosan supported on porous glass beads as a new green adsorbent for heavy metal recovery, Chemical Engineering Journal, 229 (2013) 217-224.

[16] W.S. Wan Ngah, L.C. Teong, M.A.K.M. Hanafiah, Adsorption of dyes and heavy metal ions by chitosan composites: A review, Carbohydrate Polymers, 83 (2011) 1446-1456.

[17] J.-H. Xu, H. Zhao, W.-J. Lan, G.-S. Luo, A Novel Microfluidic Approach for Monodispersed Chitosan Microspheres with Controllable Structures, Advanced Healthcare Materials, 1 (2012) 106-111.

[18] J. Xu, X. Xu, H. Zhao, G. Luo, Microfluidic preparation of chitosan microspheres with enhanced adsorption performance of copper(II), Sensors and Actuators B: Chemical, 183 (2013) 201-210.

[19] V. Singh, A.K. Sharma, D.N. Tripathi, R. Sanghi, Poly(methylmethacrylate) grafted chitosan: An efficient adsorbent for anionic azo dyes, Journal of Hazardous Materials, 161 (2009) 955-966.

[20] V. Singh, A.K. Sharma, R. Sanghi, Poly(acrylamide) functionalized chitosan: An efficient adsorbent for azo dyes from aqueous solutions, Journal of Hazardous Materials, 166 (2009) 327-335.

[21] Y. Zhu, Z. Bai, W. Luo, B. Wang, L. Zhai, A facile ion imprinted synthesis of selective biosorbent for Cu2+ via microfluidic technology, Journal of Chemical Technology & Biotechnology, 92 (2017) 2009-2022.

[22] Y. Zhu, Z. Bai, B. Wang, L. Zhai, W. Luo, Microfluidic synthesis of renewable biosorbent with highly comprehensive adsorption performance for copper (II), Frontiers of Chemical Science and Engineering, 11 (2017) 238-251.

[23] S.-T. Lee, F.-L. Mi, Y.-J. Shen, S.-S. Shyu, Equilibrium and kinetic studies of copper(II) ion uptake by chitosan-tripolyphosphate chelating resin, Polymer, 42 (2001) 1879-1892.

[24] T.C. Coelho, R. Laus, A.S. Mangrich, V.T. de Fávere, M.C.M. Laranjeira, Effect of heparin coating on epichlorohydrin cross-linked chitosan microspheres on the adsorption of copper (II) ions, Reactive and Functional Polymers, 67 (2007) 468-475.

[25] B. Wang, Y. Zhu, Z. Bai, R. Luque, J. Xuan, Functionalized chitosan biosorbents with ultra-high performance, mechanical strength and tunable selectivity for heavy metals in wastewater treatment, Chemical Engineering Journal, 325 (2017) 350-359.

[26] M.J. Frisch, G.W. Trucks, H.B. Schlegel, G.E. Scuseria, M.A. Robb, J.R. Cheeseman, G. Scalmani, V. Barone, B. Mennucci, G.A. Petersson, H. Nakatsuji, M. Caricato, X. Li, H.P. Hratchian, A.F. Izmaylov, J. Bloino, G. Zheng, J.L. Sonnenberg, M. Hada, M. Ehara, K. Toyota, R. Fukuda, J. Hasegawa, M. Ishida, T. Nakajima, Y. Honda, O. Kitao, H. Nakai, T. Vreven, J.A.M. Jr., J.E. Peralta, F. Ogliaro, M. Bearpark, J.J. Heyd, E. Brothers, K.N. Kudin, V.N. Staroverov, T. Keith, R. Kobayashi, J. Normand, K. Raghavachari, A. Rendell, J.C. Burant, S.S. Iyengar, J. Tomasi, M. Cossi, N. Rega, J.M. Millam, M. Klene, J.E. Knox, J.B. Cross, V. Bakken, C. Adamo, J. Jaramillo, R. Gomperts, R.E. Stratmann, O. Yazyev, A.J. Austin, R. Cammi, C. Pomelli, J.W. Ochterski, R.L. Martin, K. Morokuma, V.G. Zakrzewski, G.A. Voth, P. Salvador, J.J. Dannenberg, S. Dapprich, A.D. Daniels, O. Farkas, J.B. Foresman, J.V. Ortiz, J. Cioslowski, D.J. Fox, Gaussian 09, Revision C.01,Gaussian, Inc., Wallingford CT, in, 2010.

[27] R.H. Hertwig, W. Koch, On the parameterization of the local correlation functional. What is Becke-3-LYP?, Chemical Physics Letters, 268 (1997) 345-351.

[28] R. Krishnan, J.S. Binkley, R. Seeger, J.A. Pople, Self‐consistent molecular orbital methods. XX. A basis set for correlated wave functions, The Journal of Chemical Physics, 72 (1980) 650-654.

[29] W.R. Wadt, P.J. Hay, Ab initio effective core potentials for molecular calculations - potentials for the transition-metal atoms Sc to Hg, The Journal of Chemical Physics, 82 (1985) 270-283.

[30] R. Ghiasi, E. Ebrahimi Mokaram, Natural Bond Orbital (NBO) Population Analysis of Iridabenzene (C5H5Ir)(PH3)3, Journal of Applied Chemical Research, 6 (2012) 7-13.

[31] S.K. Parida, S. Sahu, S. Sharma, Interaction of third-row main group dicarbides, C2X (X=K–Br) with molecular oxygen: A density functional study, Computational and Theoretical Chemistry, 1032 (2014) 1-6.

[32] B. Wang, P. Prinsen, H. Wang, Z. Bai, H. Wang, R. Luque, J. Xuan, Macroporous materials: microfluidic fabrication, functionalization and applications, Chemical Society Reviews, 46 (2017) 855-914.

[33] W.J. Weber, J.C. Morris, Kinetics of adsorption on carbon from solution, Journal of the Sanitary Engineering Division, 89 (1963) 31-60.

[34] A.E. Ofomaja, Intraparticle diffusion process for lead(II) biosorption onto mansonia wood sawdust, Bioresource Technology, 101 (2010) 5868-5876.

[35] B.H. Hameed, M.I. El-Khaiary, Malachite green adsorption by rattan sawdust: Isotherm, kinetic and mechanism modeling, Journal of Hazardous Materials, 159 (2008) 574-579.

[36] J. Pan, H. Yao, X. Li, B. Wang, P. Huo, W. Xu, H. Ou, Y. Yan, Synthesis of chitosan/γ-Fe2O3/fly-ash-cenospheres composites for the fast removal of bisphenol A and 2,4,6-trichlorophenol from aqueous solutions, Journal of Hazardous Materials, 190 (2011) 276-284.

[37] Y.C. Wong, Y.S. Szeto, W.H. Cheung, G. McKay, Equilibrium Studies for Acid Dye Adsorption onto Chitosan, Langmuir, 19 (2003) 7888-7894.

[38] T.W. Weber, R.K. Chakravorti, Pore and solid diffusion models for fixed-bed adsorbers, AIChE Journal, 20 (1974) 228-238.

[39] S.J. Allen, G. McKay, J.F. Porter, Adsorption isotherm models for basic dye adsorption by peat in single and binary component systems, Journal of Colloid and Interface Science, 280 (2004) 322-333.

[40] J. Karuga, Y.A. Jande, H.T. Kim, C.K. King'ondu, Fish Swim Bladder-Derived Porous Carbon for Defluoridation at Potable Water pH, Science, 6 (2016) 500-514.

[41] M. Jain, V.K. Garg, K. Kadirvelu, Chromium(VI) removal from aqueous system using Helianthus annuus (sunflower) stem waste, Journal of Hazardous Materials, 162 (2009) 365-372.

[42] J.G. Speight, Lange's Handbook of Chemistry, 16th ed., McGRAW-HILL, New York, 2005.

[43] P.X. Sheng, Y.-P. Ting, J.P. Chen, Biosorption of Heavy Metal Ions (Pb, Cu, and Cd) from Aqueous Solutions by the Marine Alga Sargassum sp. in Single- and Multiple-Metal Systems, Industrial & Engineering Chemistry Research, 46 (2007) 2438-2444.

[44] N.C. Braier, R.A. Jishi, Density functional studies of Cu2+ and Ni2+ binding to chitosan, Journal of Molecular Structure: THEOCHEM, 499 (2000) 51-55.

[45] A.S. Portnyagin, S.Y. Bratskaya, A.V. Pestov, A.V. Voit, Binding Ni(II) ions to chitosan and its N-heterocyclic derivatives: Density functional theory investigation, Computational and Theoretical Chemistry, 1069 (2015) 4-10.

[46] B. Hassan, V.K. Rajan, V.M.A. Mujeeb, M. K, A DFT based analysis of adsorption of Hg2+ ion on chitosan monomer and its citralidene and salicylidene derivatives: Prior to the removal of Hg toxicity, International Journal of Biological Macromolecules, 99 (2017) 549-554.

[47] B. Hassan, K. Muraleedharan, V.M. Abdul Mujeeb, Density functional theory studies of Pb (II) interaction with chitosan and its derivatives, International Journal of Biological Macromolecules, 74 (2015) 483-488.

[48] O. Gutten, L. Rulíšek, Predicting the Stability Constants of Metal-Ion Complexes from First Principles, Inorganic Chemistry, 52 (2013) 10347-10355.

[49] I. Rajaei, S.N. Mirsattari, Spectroscopic characteristic (FT-IR, 1H, 13C NMR and UV–Vis) and theoretical calculations (MEP, DOS, HOMO-LUMO, PES, NBO analysis and keto‑enol tautomerism) of new tetradentate N,N′-bis(4-hydroxysalicylidene)-1,4-phenylenediamine ligand as chelating agent for the synthesis of dinuclear Co(II), Ni(II), Cu(II) and Zn(II) complexes, Journal of Molecular Structure, 1163 (2018) 236-251.

[50] B. Kosar, C. Albayrak, Spectroscopic investigations and quantum chemical computational study of (E)-4-methoxy-2-[(p-tolylimino)methyl]phenol, Spectrochimica Acta Part A: Molecular and Biomolecular Spectroscopy, 78 (2011) 160-167.

[51] E. Scrocco, J. Tomasi, Electronic Molecular Structure, Reactivity and Intermolecular Forces: An Euristic Interpretation by Means of Electrostatic Molecular Potentials, in: P.-O. Löwdin (Ed.) Advances in Quantum Chemistry, Academic Press, 1978, pp. 115-193.

[52] N.T. Abdel-Ghani, A.M. Mansour, M.F. Abo El-Ghar, O.M. El-Borady, H. Shorafa, Co(II), Ni(II) and Cu(II) complexes of azo-aminopyrazole ligand: Spectroscopic, crystal structure and quantum chemical calculations, Inorganica Chimica Acta, 435 (2015) 187-193.

[53] N. Hasani, M. Najim Abid AL-jibouri, Synthesis, characterization, and DFT study of some transition metal complexes with Schiff base derived from 2-acetylthiophene and l-methionine, Research on Chemical Intermediates, 43 (2017) 4585-4610.

[54] F.A.A. Mulder, M. Filatov, NMR chemical shift data and ab initio shielding calculations: emerging tools for protein structure determination, Chemical Society Reviews, 39 (2010) 578-590.